Journal of Solid State Chemistry 182 (2009) 3098–3104

Contents lists available at ScienceDirect

Journal of Solid State Chemistry

journal homepage: www.elsevier.com/locate/jssc

Direct low-temperature synthesis of RB_6 (R=Ce, Pr, Nd) nanocubes and nanoparticles

Maofeng Zhang [a,b,*], Xiaoqing Wang [b], Xianwen Zhang [b], Pengfei Wang [b], Shenglin Xiong [b], Liang Shi [b], Yitai Qian [b,**]

[a] Section 503, Xi'an High Technique Institute, Xi'an 710025, China
[b] Hefei National Laboratory for Physical Sciences at Microscale, Department of Chemistry, University of Science and Technology of China, Jinzhai Road 96, Hefei 230026, China

ARTICLE INFO

Article history:
Received 14 June 2009
Received in revised form
25 August 2009
Accepted 30 August 2009
Available online 9 September 2009

Keywords:
*R*B6
Low-temperature
Nanocubes
Nanoparticles

ABSTRACT

Rare-earth hexaborides (RB_6, R=Ce, Pr, Nd) nanocrystals were prepared by a facile solid state reaction in an autoclave. Single-crystalline RB_6 nanocubes were fabricated at 500 °C starting from B_2O_3, $RCl_3 \cdot 6H_2O$ and Mg powder. RB_6 nanoflakes and nanoparticles could be obtained around 400 °C using $NaBH_4$ as boron resource. XRD patterns show that all of the hexaborides are cubic phase with high crystallinity and high purity and have lattice parameters that are consistent with nearly stoichiometric products. Raman spectra elucidate the active vibrational modes of the hexaborides. The TEM and FESEM images clearly show that the nanocubes have an average size of 200 nm and nanoparticles of 30 nm. Our experiment developed an efficient, simple and low-cost route to prepare RB_6, which could be extended further to the preparation of other rare-earth metal hexaborides.

1. Introduction

Rare-earth hexaborides (RB_6) (R=La, Ce, Pr, Nd, etc.) have attracted much attention because of their various peculiar properties such as high melting point, high hardness, high chemical stability, superconductivity [1,2], magnetic properties [3–5], high efficiency thermionic emission and narrow band semiconductivity, and so on [6–10]. Therefore, rare-earth hexaborides possess great technical importance. In the rare-earth hexaborides family, LaB_6 and CeB_6 are used as an electron source with high brightness and longevity. Compared with LaB_6 (work function ~2.72 eV), CeB_6 has a lower work function (~2.5 eV) and a lower volatility, which means lower operation temperature and longer service life when used as a thermionic electron emitter [11,12]. It has been reported that PrB_6 (work function ~3.12 eV) [13] might be a viable cathode material as well as LaB_6, which has substantial practical application [14].

Previously, RB_6 has been synthesized by various methods, such as direct solid phase reaction of lanthanide or its oxides with elemental boron around 1800 °C [1,15–17]; the floating zone method of rare-earth oxides with boron at 1700 °C [5,18,19]; high-pressure and high temperature synthesis from rare-earth oxides and boron at 1600 °C [20]; carbothermal reduction of lanthanide oxide and boron at 1500 °C [21]; solution method in molten aluminum at about 1300 °C [22]; chemical vapor deposition (CVD) method around 1150 °C [7,8,23]; salt electrolysis at 850 °C [24]; pulsed laser deposition (PLD) technique at 850 °C [25]. Recently, submicron-sized rare-earth hexaborides were synthesized at a relatively low-temperature of 900 °C using metal acetate precursors [26]. Since the properties of a nanostructured material can be significantly changed by quantum effects, it is expected that nanostructure RB_6, such as nanowires [7,8,27] and nanoobelisks [28], can give rise to exceptional properties. Nevertheless, most previous methods for the preparation of rare-earth hexaborides need either high-temperature or harsh reaction conditions. Researchers are exploring low reaction temperature, low cost, simple and convenient synthetic methods for the preparation of these compounds.

However, to our knowledge, few papers on the preparation of rare-earth hexaborides synthesized at the temperature as low as 400 °C have been reported as yet. In the present study, we report a simple low-temperature synthesis of RB_6 (R=Ce, Pr, Nd) nanocrystals by a facile solid state reactions in an autoclave. It is worth noting that one feature of this synthesis route is the high pressure in the autoclave, coming from the produced H_2 during the reaction (about 50 atm in reaction equation (1) and 100 atm in reaction equation (2), estimated by the ideal gas law). The

* Corresponding author at: Hefei National Laboratory for Physical Sciences at Microscale, Department of Chemistry, University of Science and Technology of China, Jinzhai Road 96, Hefei 230026, China.
** Corresponding author.
E-mail addresses: mfzhang@ustc.edu.cn (M. Zhang), ytqian@ustc.edu.cn (Y. Qian).

0022-4596/$ - see front matter © 2009 Elsevier Inc. All rights reserved.
doi:10.1016/j.jssc.2009.08.032

reaction equations can be described as follows:

$$RCl_3 \cdot 6H_2O(s) + 3B_2O_3(s) + 16.5Mg(s) = RB_6(s) + 1.5MgCl_2(s) + 15MgO(s) + 6H_2(g) \quad (1)$$

$$RCl_3 \cdot 6H_2O(s) + 6NaBH_4(s) + 3Mg(s) = RB_6(s) + 3NaCl(s) + 3MgO(s) + 3NaOH(s) + 16.5H_2(g) \quad (2)$$

X-ray diffraction (XRD), energy dispersive X-ray (EDX) spectroscopy and Raman spectra were used to confirm the structures and compositions of RB_6. The morphologies of the products were characterized by field-emission scanning electron microscope (FESEM) and transmission electron microscope (TEM).

2. Experimental section

2.1. Sample preparation

Preparation of RB_6 (R=Ce, Pr, Nd) nanocubes: In a typical procedure, an appropriate amount of $RCl_3 \cdot 6H_2O$ (0.003 mol), B_2O_3 (0.009 mol), and excessive Mg (0.075 mol) were put into a stainless steel autoclave of 25 ml capacity. Then, the autoclave was sealed under Ar atmosphere and maintained at 500 °C for 12 h, followed by naturally cooling to room temperature. The product was washed with dilute hydrochloric acid and distilled water, respectively, to remove MgO, $MgCl_2$ and other impurities. The final products were vacuum-dried at 60 °C for 4 h.

Preparation of RB_6 (R=Ce, Pr, Nd) nanoparticles: In a typical procedure, an appropriate amount of $RCl_3 \cdot 6H_2O$ (0.003 mol), excessive $NaBH_4$ (0.025 mol), and excessive Mg (0.040 mol) were put into a stainless steel autoclave of 25 ml capacity. Then, the autoclave was sealed under Ar atmosphere and maintained at 400 °C for 48 h, followed by naturally cooling to room temperature. The products were washed with dilute hydrochloric acid and distilled water, respectively, to remove NaOH, MgO, NaCl, and other impurities. The final products were vacuum-dried at 60 °C for 4 h.

2.2. Characterization

The phase and composition of the products were determined by a Rigaku D/Max-γA rotating-anode X-ray diffractometer equipped with monochromatic high-intensity CuKα radiation (λ=1.54178 Å). The morphologies of the samples were observed with a transmission electron microscope (JEOL-2010) with an attached energy dispersive X-ray spectroscopy system, having an accelerating voltage of 200 kV with a tungsten filament. Field-emission scanning electron microscope images were taken on a JEOL JSM-6300F SEM. Raman spectra were measured on a LABRAM-HR Raman spectrophotometer. The 514.5-nm laser was used as an excitation light source.

3. Results and discussion

3.1. Morphology and structure of the samples

XRD analysis was used to determine the structure and phase of the samples. Fig. 1 shows XRD patterns of the RB_6 nanocubes obtained by Eq. (1). All the peaks can be readily indexed to cubic crystal system [space group: $Pm3m$ (221)] of RB_6 with calculated lattice constants a=4.136 ± 0.001 Å (CeB_6); 4.125 ± 0.001 Å (PrB_6); and 4.119 ± 0.001 Å (NdB_6), which is very close to the reported data (JCPDS card nos.: 79-2163; 25-1455; 11-0087). No characteristic peaks of impurities were detected. The strong and sharp reflection peaks disclose that the as-prepared nanocrystals are all well crystallized.

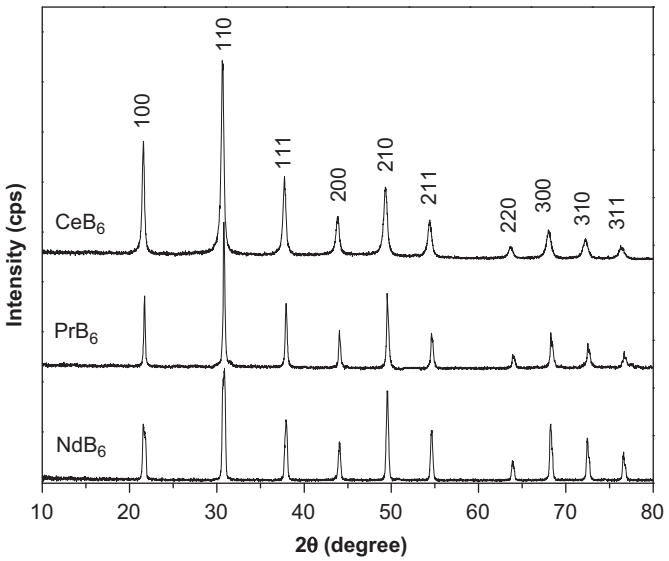

Fig. 1. Typical XRD patterns of the RB_6 nanocubes prepared at 500 °C for 12 h.

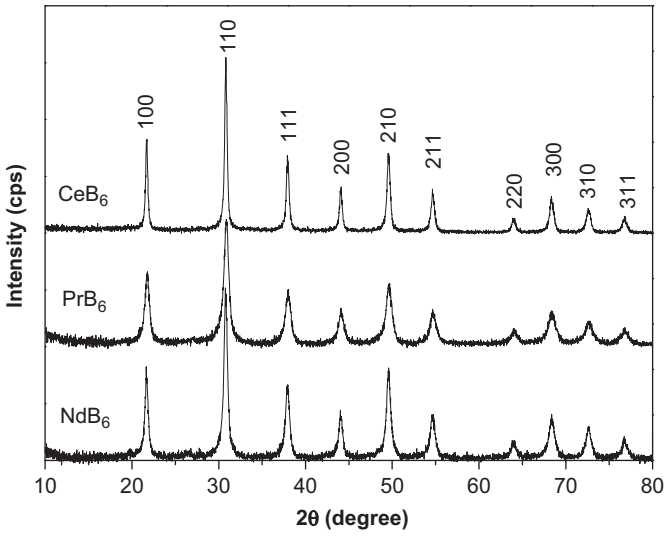

Fig. 2. Typical XRD patterns of the RB_6 nanoparticles prepared around 400 °C for 12 h.

Fig. 2 shows the XRD patterns of the RB_6 nanoparticles prepared by Eq. (2). All the reflection peaks of the products can be easily indexed to cubic structure with calculated lattice constants a=4.135 ± 0.001 Å (CeB_6); 4.126 ± 0.001 Å (PrB_6); and 4.119 ± 0.001 Å (NdB_6), which are in good agreement with the literature values (JCPDS card nos.: 11-0670; 25-1455; 11-0087). No other impurity peaks were detected, indicating the high purity of as-obtained samples.

Energy dispersive X-ray (EDX) spectroscopy was used to characterize the composition of the products. EDX analysis of CeB_6 samples reveals the presence of Ce and B for CeB_6 nanocubes (Fig. 3a) and CeB_6 nanoparticles (Fig. 3b), and the elements of Ce and B are dominant in the materials. The other elements detected in the samples originate from copper grids and the absorption of oxygen on the powder surface. Similar results are found in samples of RB_6 (R=Pr, Nd) nanocubes and nanoparticles.

The morphologies and microstructure of the samples were examined by FESEM and TEM. Fig. 4a–c shows the FESEM images

of nanocrystalline RB_6 prepared at 500 °C for 12 h. It is evident that some particles have the shape of rectangular prisms, others as cubes. The particle size distribution ranges from 160 to 220 nm by measuring the size of a large number of well defined particles. The average particle size is about 200 nm. It is named as "nanocubes" in the present work. Take CeB_6 for example, TEM images of CeB_6 nanocubes obtained at different reaction temperatures and times are shown in Fig. 5a–c. CeB_6 nanocubes were formed at 500 °C for 12 h (Fig. 5a). The inset ED pattern of the selected area taken along the $<001>$ zone axis indicates its single-crystalline nature of individual CeB_6 nanocube. Varying reaction time between 12 and 48 h did not significantly affect the size and morphology of CeB_6 nanocubes (Fig. 5b). If reaction time was shorter than 4 h, the reaction became very incomplete and the crystallinity was very poor due to too short reaction time.

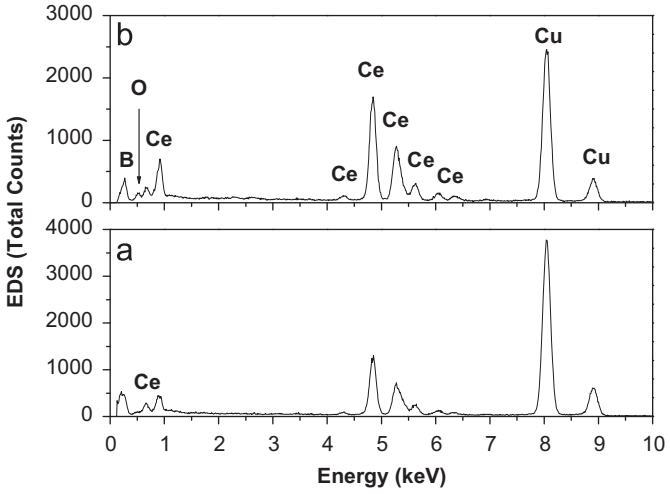

Fig. 3. EDX spectra of (a) CeB_6 nanoparticles and (b) CeB_6 nanocubes on TEM copper grid.

At 450 °C, only a small amount of RB_6 could be obtained. However, if the reaction temperature increases to 600 °C, the particle size increases (Fig. 5c). The optimum reaction temperature is 500 °C and large-amount of RB_6 could be obtained under this temperature.

The crystal growth mechanisms of the hexaboride nanocubes have been explained on the basis of TEM images and XRD observations. At initial stage, it produces amorphous product. This amorphous product acts as the nucleation center for the formation of hexaboride cubes. It converts into small crystalline primary particles at the elevated temperature. Finally, the crystalline primary particles are joined together to form nano-sized crystals, followed by a 3D-oriented attachment [29]. Ultimately, the cubic crystals are obtained at 500 °C. The explanation is based on the following: The final shape of the particles is decided by two different crystalline phases, {100} and {111}, where the {111} phase has a higher surface energy than the {100} phase. Therefore, at higher temperatures the {111} phase has gained more thermal energy, which leads to the formation of the most stable phase of the cubic morphology.

Fig. 6a–c shows typical TEM images of the RB_6 (R=Ce, Pr, Nd) samples prepared by using reaction equation (2). Nanoflakes were prepared at 420 °C for CeB_6, PrB_6, and NdB_6. The inset selected-area electron diffraction (SAED) pattern obtained from a random aggregate of nanocrystalline CeB_6 indicates its high crystallinity. These concentric rings can all be assigned to the cubic phase of CeB_6, which is consistent with XRD pattern. In our previous work [30], however, LaB_6 nanoparticles with average particle size of 30 nm could be obtained at 400 °C for 12 h.

In the present preparation process, it is found that the reaction temperature and time play important roles in the formation of different morphologies of RB_6, such as nanoflakes and nanoparticles. To understand the formation mechanism of these morphologies, we take CeB_6 samples for example. Fig. 7a–c shows the TEM images and ED patterns of the nanocrystalline CeB_6 prepared at 420 °C for 8, 24 and 48 h, respectively. At initial stage, nanocrystallites with a mean grain size of 3 nm were formed

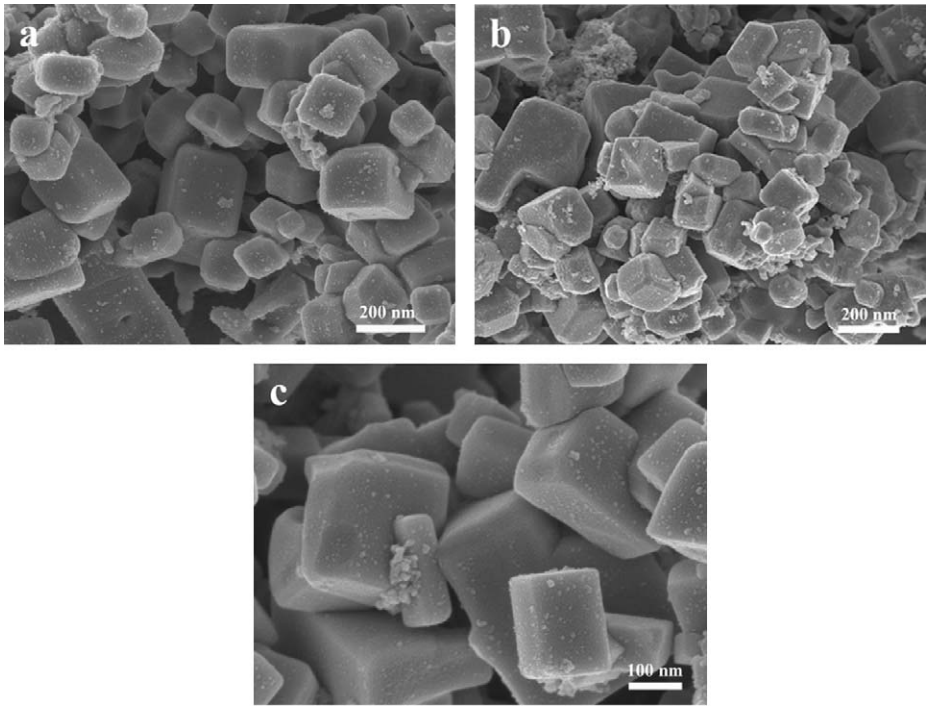

Fig. 4. FESEM images of RB_6 nanocubes prepared at 500 °C for 12 h (a) CeB_6, (b) PrB_6, and (c) NdB_6.

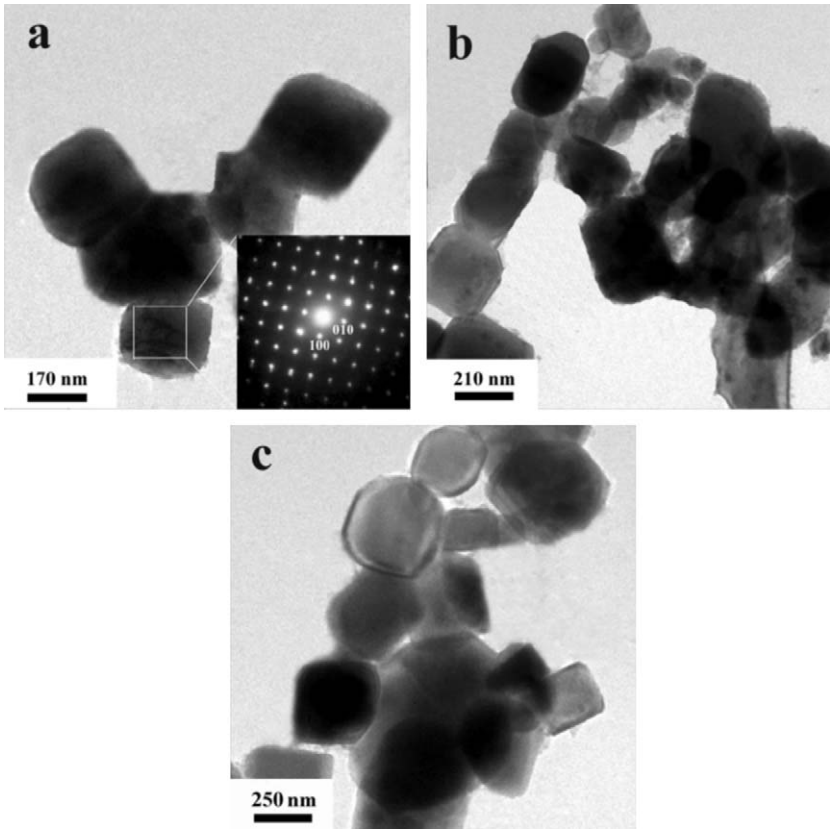

Fig. 5. TEM images of the CeB_6 nanocubes prepared at (a) 500 °C for 12 h (inset: SAED pattern), (b) 500 °C for 24 h, (c) 600 °C for 12 h.

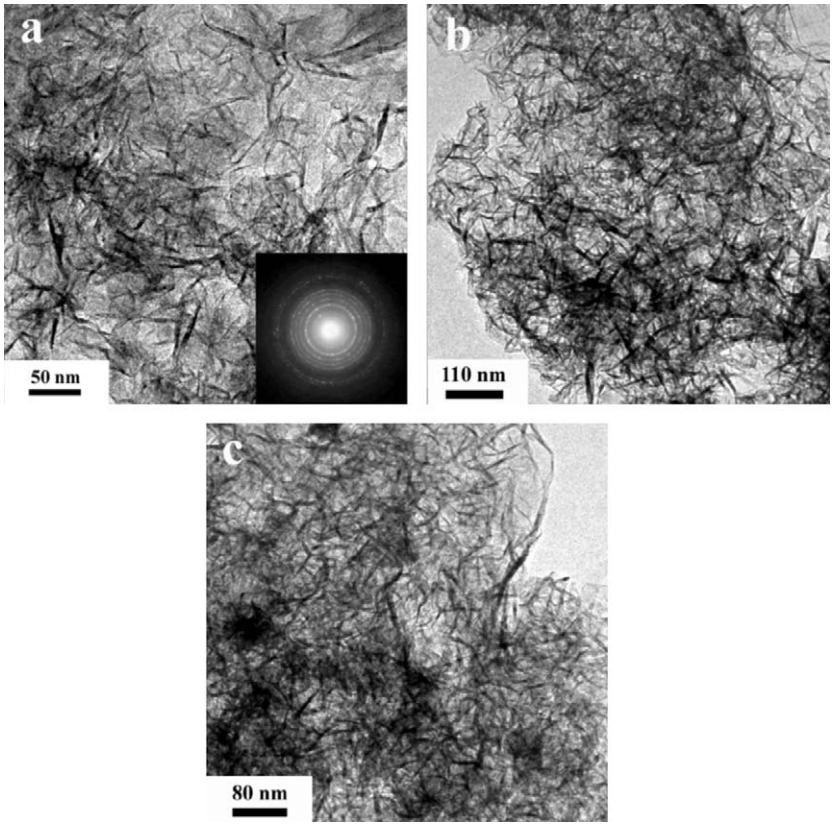

Fig. 6. TEM images and corresponding ED patterns of nanocrystalline RB_6 prepared at 420 °C for 12 h (a) CeB_6, (b) PrB_6, and (c) NdB_6.

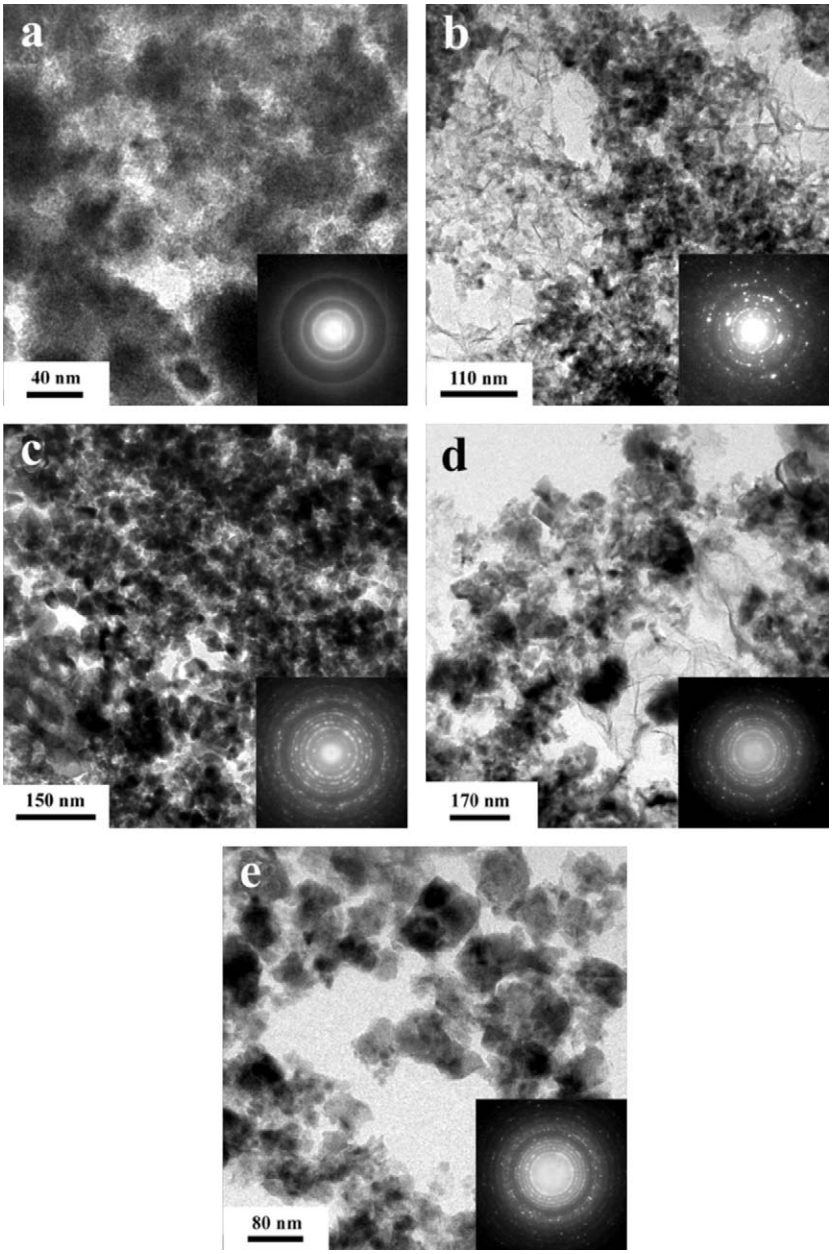

Fig. 7. TEM images and corresponding ED patterns of the nanocrystalline CeB_6 prepared at (a) 420 °C for 8 h, (b) 420 °C for 24 h, (c) 420 °C for 48 h, (d) 500 °C for 12 h, and (e) 600 °C for 12 h.

(Fig. 7a). After reacted for 12 h, nanoflakes were obtained (Fig. 6b). When reaction time was extended to 24 h, as shown in Fig. 7b, nanoflakes almost disappeared and turned into nanoparticles. After 48 h (Fig. 7c), CeB_6 nanoparticles with an average size of about 30 nm were fabricated. Form Fig. 7a–c, it was found that the corresponding ED patterns indicating the crystallinity of the samples was improved gradually due to the increases of reaction duration. On the other hand, a higher temperature favored the formation of CeB_6 nanoparticles. At 500 °C, the dominant products were nanoparticles and only a small amount of nanoflakes could be observed, as shown in Fig. 7d. At 600 °C, nanoflakes disappeared and CeB_6 nanoparticles were formed (Fig. 7e). Nevertheless, no CeB_6 could be obtained below 350 °C.

The main question remaining is why the crystals grow in the form of nanoparticles rather than nanocubes when $NaBH_4$ was used instead of B_2O_3. It is found that the reactants whether in the liquid or gaseous state play a crucial role in determining the shape of the final product. In the preparation of RB_6 nanocubes, as Eq. (1) described, B_2O_3 begins to turn into liquid (melting point 450 °C) in the heating process. With the increase of temperature, more liquid B_2O_3 coats the RCl_3 and produces RB_6 nanocubes. In the process to RB_6 nanoparticles by reacting RCl_3 with $NaBH_4$, as Eq. (2) described. The reaction (Eq. (2)) is thermodynamically spontaneous and exothermic. When the heating temperature is 420 °C, the inner temperature in the autoclave may be higher than 500 °C. $NaBH_4$ begins to decompose acutely when the temperature is above 500 °C as expressed in Eq. (3). The gaseous BH_3 and NaH react further with RCl_3 and produce RB_6 nanoparticles. Because of gaseous BH_3 reacting with RCl_3, it first forms 3 nm grains (Fig. 7a). With increases of reaction time from 12 to 48 h, the products converts from 3 nm grains into nanoflakes, and

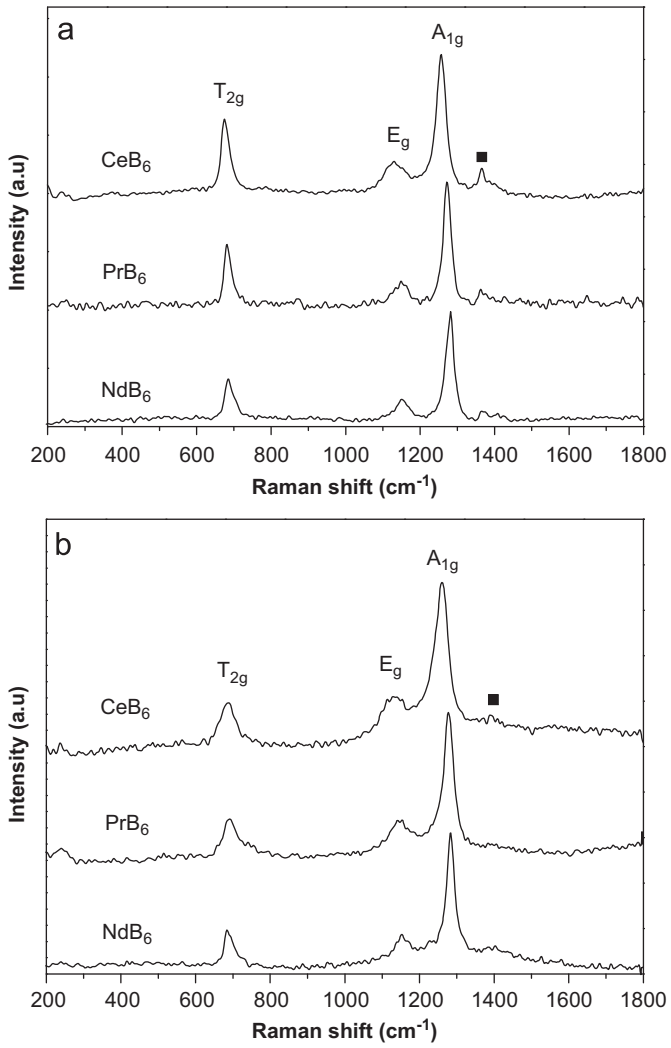

Fig. 8. Raman spectra of (a) RB_6 nanocubes and (b) RB_6 nanoparticles measured at room temperature in ambient.

ultimately size of 30 nm nanoparticles:

$$NaBH_4 \rightarrow NaH + BH_3 \quad (3)$$

3.2. Raman spectra of the products

It is well-known that Raman spectra are an important tool for identifying the lattice dynamics and the crystal electric field splitting of rare-earth hexaborides. Fig. 8 shows Raman spectra of RB_6 nanocubes and nanoparticles, respectively. According to group theory [31], the hexaborides structure has a $Pm3m$ cubic symmetry, which contains $A_{1g}+E_g+T_1g+T_{2g}+2T_{1u}+T_{2u}$ vibrational modes, where A_{1g}, E_g, and T_{2g} are Raman active phonons. The A_{1g} and E_g modes originate from the stretching vibration of B–B bonds and T_{2g} is due to the valence angle bending of B–B–B in the boron lattice. It can be seen that these spectra are shifted along the vertical direction, and the order corresponds to the decrease of the lattice constants of RB_6 from the top to bottom. However, the peaks of Raman spectra of the same compound of RB_6 nanocubes and nanoparticles remain unchanged in the present experiment. The three expected main peaks are observed around 680 cm^{-1} (T_{2g}), 1140 cm^{-1} (E_g) and 1260 cm^{-1} (A_{1g}), which are in agreement with earlier reports [32–34], and they completely satisfy the polarization selection rule in the cubic symmetry. These three prominent peaks are additional confirmation for the formation of hexaborides because the peaks obey the selection rule for the hexaborides' cubic symmetry. A broad peak around 1400 cm^{-1}, labeled as ■, is commonly observed with a relatively strong intensity for trivalent and intermediate-valent crystals [35]. For trivalent case, twice the energy of T_{2g} is slightly lower than the peak energy, however, the peak energy systematically follows twice the energy of T_{2g}. In LaB_6, the peak energy is far from twice the energy of T_{2u} and that of T_{2g} is very close to the peak energy. For SmB_6 the energy coincidence is very good. Thus it can be concluded that the peak observed in the trivalent case originates from the second-order process of T_{2g}.

4. Conclusions

In summary, this work presents a simple and efficient approach for the preparation of RB_6 nanocubes at 500 °C and RB_6 nanoparticles around 400 °C. The XRD patterns, EDX spectra and Raman spectra confirm the high crystallinity, high purity and the single phase of the products. The TEM and FESEM images clearly show that the products are nanocubes with an average size of 200 nm, and nanoparticles with an average size of 30 nm. Compared with previous routes, the present route has the advantages of mildness, simplicity and low cost. This method opens the prospect of using cheap reactants for the synthesis of other metal hexaborides.

Acknowledgments

This work was supported by the National Natural Science Foundation of China (no. 20431020), the 973 Project of China (no. 2005CB623601), the China Postdoctoral Science Foundation Funded Project (no. 20080440708), and the Natural Science Basic Research Plan in Shanxi Province of China (no. 2009JQ2012).

References

[1] K. Hiebl, M.J. Sienko, Inorg. Chem. 19 (1980) 2179.
[2] I. Bat'Ko, M. Bat'Kova, K. Flachbart, J. Alloys Compd. 217 (1995) 11.
[3] H. Hacker, Y. Shimada, K.S. Chung, Phys. Status Solidi A 4 (1970–1996) 459.
[4] J.R. Shannon, M.J. Sienko, Inorg. Chem. 11 (1972) 904.
[5] K. Takahashi, S. Kunii, J. Solid State Chem. 133 (1997) 198.
[6] E.L. Kerley, C.D. Hanson, D.H. Russell, Anal. Chem. 62 (1990) 409.
[7] H. Zhang, Q. Zhang, J. Tang, L.C. Qin, J. Am. Chem. Soc. 127 (2005) 2862.
[8] H. Zhang, J. Tang, Q. Zhang, G. Zhao, G. Yang, J. Zhang, O. Zhou, L.C. Qin, Adv. Mater. 18 (2006) 87.
[9] A.E. Baranovskiy, G.E. Grechnev, A.V. Logosha, I.V. Svechkarev, V.B. Filippov, N.Y. Shitsevalova, O.J. Zogał, O. Eriksson, Phys. Status Solidi C 3 (2006) 229.
[10] M. Takeda, T. Fukuda, F. Domingo, T. Miura, J. Solid State Chem. 177 (2004) 471.
[11] L.W. Swanson, D.R. McNeely, Surf. Sci. 83 (1979) 11.
[12] P.R. Davis, M.A. Gesley, G.A. Schwind, L.W. Swanson, Appl. Surf. Sci. (1989) 381.
[13] S.V. Meschel, O.J. Kleppa, J. Alloys Compd. 221 (1995) 37.
[14] W.D. Richard, W.S. Dean, J. Appl. Phys. 26 (1955) 1004.
[15] J.M. Lafferty, J. Appl. Phys. 22 (1951) 299.
[16] B.J. Curtis, H. Graffenberger, Mater. Res. Bull. 1 (1966) 27.
[17] J.R. Rea, E. Kostiner, J. Cryst. Growth 11 (1971) 110.
[18] S. Otani, H. Nakagawa, Y. Nishi, N. Kieda, J. Solid State Chem. 154 (2000) 238.
[19] S. Otani, M.M. Korsukova, T. Mitsuhashi, N. Kieda, J. Cryst. Growth (2000) 378.
[20] X.D. Zhao, X.Y. Liu, F. Lin, W.N. Liu, W.H. Su, J. Alloys Compd. 249 (1997) 247.
[21] B. Post, D. Moskowitz, F.W. Glaser, J. Am. Chem. Soc. 78 (1956) 1800.
[22] V.V. Gurin, M.M. Korsukova, S.P. Nikanorov, I.A. Smirnov, N.N. Stepanov, S.G. Shulman, J. Less-Common Met. 67 (1979) 115.
[23] Q.Y. Zhang, J.Q. Xu, Y.M. Zhao, H.J. Xiao, P.L. Shu, Adv. Funct. Mater. (2009) 5.
[24] M. Kamaludeen, I. Selvaraj, A. Visuvasama, R. Jayavel, J. Mater. Chem. 8 (1998) 2205.

[25] V. Craciun, D. Craciun, Appl. Surf. Sci. 247 (2005) 384.
[26] R.K. Selvan, I. Genish, I. Perelshtein, J.M.C. Moreno, A. Gedanken, J. Phys. Chem. C 112 (2008) 1795.
[27] H. Zhang, Q. Zhang, G.P. Zhao, J. Tang, O. Zhou, L.C. Qin, J. Am. Chem. Soc. 127 (2005) 13120.
[28] J.R. Brewer, N. Deo, Y.M. Wang, C.L. Cheung, Chem. Mater. 19 (2007) 6379.
[29] J.J. Teo, Y. Chang, H.C. Zeng, Langmuir 22 (2006) 7369.
[30] M.F. Zhang, L. Yuan, X.Q. Wang, H. Fan, X.Y. Wang, X.Y. Wu, H.Z. Wang, Y.T. Qian, J. Solid State Chem. 181 (2008) 294.
[31] N. Ogita, S. Nagai, N. Okamoto, F. Iga, A. Kunii, J. Akimitsu, M. Udagawa, Physica B 328 (2003) 131.
[32] P. Teredesai, D.V.S. Muthu, N. Chandrabhas, S. Meenakshi, V. Vijayakumar, P. Modak, R.S. Rao, B.K. Godwal, S.K. Sikka, A.K. Sood, Solid State Commun. 129 (2004) 791.
[33] Z. Yahia, S. Turrell, G. Turrell, J.P. Mercurio, J. Mol. Struct. 224 (1990) 303.
[34] Z. Yahia, S. Turrell, J.P. Mercurio, G. Turrell, J. Raman Spectrosc. 24 (1993) 207.
[35] N. Ogita, S. Nagai, N. Okamoto, M. Udagawa, J. Akimitsu, S. Kunii, Phys. Rev. B 68 (2003) 224305.